Studying the Efficiency of the Variational Quantum Eigensolver on the Lipkin-Meshkov-Glick Model using Quantum Machine Learning

Bendik Selvaag-Hagen, Håkon Kvernmoen

May 31, 2023

Github: https://github.com/hkve/Lipkin-Model-FYS5419/

Abstract

A Quantum Mechanical System has a Hamiltonian which takes the system and computes its eigenvalues, corresponding to the systems energies. This is an efficient way of computing the energy of a system, but is computationally hard given an complicated initial state to which one needs to find the lowest energy. This problem is classically solved either by the diagonalization of the Hamiltonian or by the Variational Method. The latter has a numerical application used in Quantum Computing called the Variational Quantum Eigensolver (VQE). Applying the VQE to a simple 2x2 Hamiltonian with a interaction and non-interaction part on one state, we achieve accurately to recreate the analytical solution from the diagonalization with varying interaction strength. Expanding the model to two qubits, the entanglement entropy of the two states is found to increase with increased interaction strength. The diagonalized Hamiltonian still correspond sufficiently to the VQE on the system. Furthermore applying the VQE to the Lipkin-Meshkov-Glick model it is far superior to that of Hartree-Fock and Random Phase Approximation. VQE is deemed to be an accurate approximation to the diagonalized Hamiltonian of the Lipkin model, with no visual deviances for a two qubit system. For a four qubit system with off-diagonal elements in the Hamiltonian, VQE struggles more and will deviate increasingly as a function of the interaction strength, although still being superior to Hartree-Fock and Random Phase Approximation.

Contents

1 Introduction 1

2 Quantum Computing 2
- 2.1 Notation . . . 2
- 2.2 Basics of Quantum Computing . . . 2
- 2.3 Pauli Encoding Hamiltonians . . . 3
- 2.4 Variational Quantum Eigensolver . . . 3
  - 2.4.1 Brief Remainder of the Variational Method . . . 3
  - 2.4.2 Algorithm . . . 4

3 Quantum Systems 4
- 3.1 $H \in \mathbb{R}^2$ Hamiltonian . . . 4
- 3.2 $H \in \mathbb{R}^4$ Hamiltonian . . . 5
- 3.3 Lipkin Model . . . 5
- 3.4 Encodings . . . 6
  - 3.4.1 Toy Hamiltonians . . . 6
  - 3.4.2 Lipkin Model . . . 7
- 3.5 Calculating density matrices . . . 7

4 Results 8
- 4.1 Toy Models . . . 8
- 4.2 Lipkin Model . . . 9

5 Discussion 9
- 5.1 Toy models . . . 9
- 5.2 Entropy . . . 10
- 5.3 Lipkin Model . . . 11
- 5.4 Future research . . . 12

6 Concluding remarks 12

7 Appendix 13
- .1 $J = 1$ Lipkin Hamiltonian . . . 13
- .2 Detailed Pauli Encoding of the Lipkin Model 13

1 Introduction

Quantum Mechanics (QM) is fundamentally hard, seeing as it has intrinsic uncertainties within, proclaimed by fundamental quantum theorems such as the Heisenberg Uncertainty Principle. Particles at such minuscule scales are not defined through classical physics, but as waves and wave-functions. To physically interpret the position and momentum of said particles need to be assessed as probability distributions. Thus it is manifestly encoded in the fabric of QM that it contains a certain amount of probabilistic features inherently in the fact that particles can not be expressed classically, but rather as states which develop.

For a Quantum Computer (QC) to be stern and act according to the probabilistic nature of the QM

realm, we need to encode each bit as a state. This requires a short introduction to Classical Computing (CC). Here, the foundation of a circuit is a rigid state, 0 or 1, which can be altered, but which remain unaltered without external signals. One can operate on these bits, often system of bits, with gates such as OR and AND, and a plethora of more operations, which creates an outcome based on whether your selection of bits are in a state 0 or 1.

Comparing this CC to a QC, the encoding is still for QC bound by having bits of values 0 or 1, although here the similarities end. Each quantum state will in an ideal world not diverge from its original value, but seeing at it is probabilistic, it will evolve and fluctuate between 0 and 1. For the sake of simplicity, we assume and ideal world where it remains in its encoded state. Each operation on the state or the collection of states has to be unitary, to retain reversibility. And most importantly, states can be in a superposition of 0 and 1, making the outcome reliant on lots of runs, seeing as the outcome is probabilistic. Two or more states can also be entangled, in a manner at which predicts with certainty the outcome of the first bit, based on the measurement on the second. These properties makes QC capable of, through different encoding and operating schemes, to solve some problems within computing better than its classical counterpart.

One of these problems is finding the ground state energy of a given quantum system. For systems without analytical solutions, the application of the variational method (VM) is common practice. Evaluating energy expectation values is computationally expensive, especially for a high number of particles. One of many algorithms developed to run on a QC is the Variational Quantum Eigensolver (VQE). We will in Section 2 introduce some key aspects of QC, in addition to an introduction to VQE. In Section 3 we will discuss the systems of which the VQE is applied, starting with two toy systems and ending with the Lipkin Model. Lastly in Section 4 and Section 5 we present and discuss our findings.

2 Quantum Computing

2.1 Notation

The basic building block of a QC is the *qbit*. Resembling the binary representation in CC, the qbit is defined as a two-level system. In the canonical/standard/Pauli basis, we express the basis states as

$$|0\rangle = \begin{pmatrix} 1 \\ 0 \end{pmatrix}, |1\rangle = \begin{pmatrix} 0 \\ 1 \end{pmatrix}.$$

Despite the similarity to bits, a qbit is allowed to be in a superposition of the two basis states, meaning that

$$|\psi\rangle = c_0 |0\rangle + c_1 |1\rangle, \qquad c_0, c_1 \in \mathbb{C}$$

is also a valid qbit, constrained to normalization $|c_0|^2 + |c_1|^2 = 1$. The modulus of the coefficients c_0, c_1 are through the Born rule interred as the point probability of measuring basis state $|0\rangle$ and $|1\rangle$ respectively, mirroring probability vectors. However, the qbits $\{|\psi\rangle_i\}$ are expressed through the coefficients $\{c_i\}$ and not their modulus, allowing both negative and complex values, resulting in the possibility for both constructive and destructive interference when added together.

We are however not only limited to a single qbit. Composite systems of two-level qbits can be created, mathematically expressed as tensor products between states. Considering the Pauli basis $\{|0\rangle, |1\rangle\}$, we can create a new basis $\{|00\rangle, |01\rangle, |10\rangle, |11\rangle\}$ through the operation

$$|ij\rangle = |i\rangle \otimes |j\rangle \qquad i, j = 0, 1. \tag{1}$$

The above procedure can be repeated for more than two qbits. In the realm of QC, the most important operators are the Pauli matrices, often referred to the X, Y and Z *gates*

$$X = \begin{pmatrix} 0 & 1 \\ 1 & 0 \end{pmatrix}, Y = \begin{pmatrix} 0 & -i \\ i & 0 \end{pmatrix}, Z = \begin{pmatrix} 1 & 0 \\ 0 & -1 \end{pmatrix} \tag{2}$$

Just as with qbits, we can through the tensor product compose operators acting on multiple qbits. To avoid potential confusion between multiple operators being applied and composite operators, a subscript on these operators will be added. For instance, a three qbit operator can be constructed as

$$X_1 Z_3 = X \otimes I \otimes Z \tag{3}$$

Where I is the 2×2 identity matrix. Here $X_1 Z_3$ applied to a three qbit state applies X to the first qbit, does nothing with the second and applies Z on the third.

2.2 Basics of Quantum Computing

In the introduction, vague outlines of the functionality of QC is presented. In this section, the circuits and representation will be presented with a elementary example of circuits and states. A Greenberger-Horne-Zeilinger(GHZ) State is a fully entangled set of three or more quantum bits, or qbits. For two qbits, this is called a Bell-state. It can be encoded by applying a Haddamard gate to the primary gate, and CNOT gates to the subsequent. In matrix representation these operations are

$$H = \begin{pmatrix} 1 & 1 \\ 1 & -1 \end{pmatrix} \qquad CNOT = \begin{pmatrix} 1 & 0 & 0 & 0 \\ 0 & 1 & 0 & 0 \\ 0 & 0 & 0 & 1 \\ 0 & 0 & 1 & 0 \end{pmatrix} \tag{4}$$

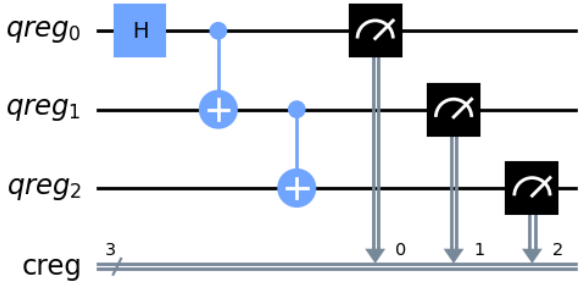

Figure 1: The circuit needed to initialize the GHZ state for three qubits.

Hadamard gates changes the basis of the gate between Pauli Z and Pauli X basis. CNOT changes the affected gate, based on the state of the control state. Visually, in a circuit, this can be presented as shown in Fig(1). The result is a full entanglement, as seen in Fig(2a), where the outcome of any measurement on any qbit, will ascertain the outcome of all other measurements, as shown in Fig(2b).

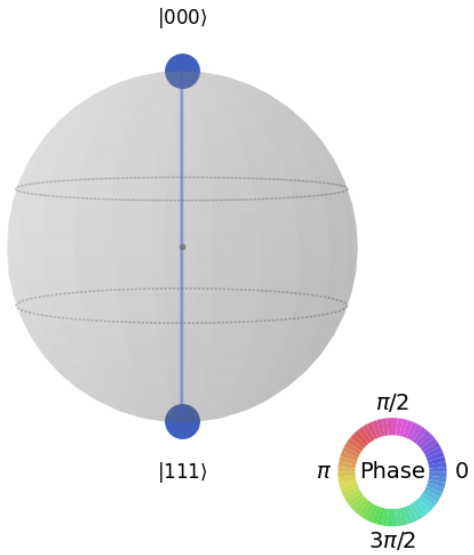

(a) The Bloch-sphere representation of the GHZ state, given three qubits. It is strictly entangled, by their parallell nature.

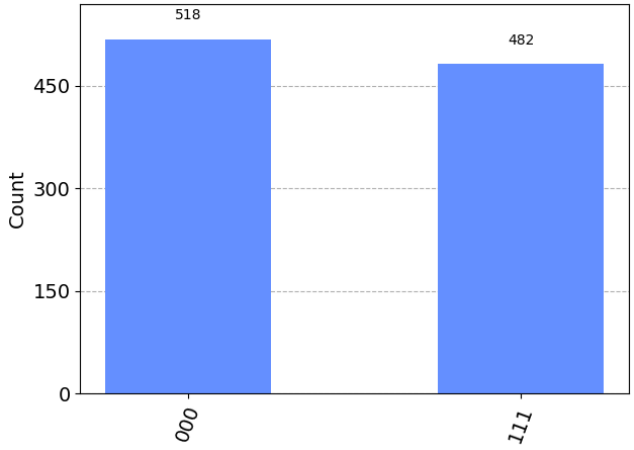

(b) The outcome of measurements of the GHZ state with three qubits.

Another important set of gates are the *rotation operators* R_x, R_y and R_z. By application to a qbit, we can reach any point on the Bloch sphere by usage of all three once. They are expressed as

$$\begin{aligned} R_x(\theta) &= e^{-iX\theta/2} = \begin{pmatrix} \cos(\theta/2) & -i\sin(\theta/2) \\ -i\sin(\theta/2) & \cos(\theta/2) \end{pmatrix}, \\ R_y(\theta) &= e^{-iY\theta/2} = \begin{pmatrix} \cos(\theta/2) & -\sin(\theta/2) \\ -\sin(\theta/2) & \cos(\theta/2) \end{pmatrix}, \\ R_z(\theta) &= e^{-iZ\theta/2} = \begin{pmatrix} e^{-i\theta/2} & 0 \\ 0 & e^{i\theta/2} \end{pmatrix} \end{aligned} \tag{5}$$

with all having a period of 4π.

2.3 Pauli Encoding Hamiltonians

To apply a specific system to VQE, the Hamiltonian must be re-written in terms of a sum of *Pauli strings*. Considering the identity I and the three Pauli matrices X, Y, Z, we construct a specific term as a tensor product of these P_i. For an n-qubit system, we require $n-1$ tensor products. Combined with a weight w_i, the Hamiltonian must be written in the from

$$H = \sum_i w_i P_i \tag{6}$$

For a general two-body Hamiltonian, this task can serve challenging. Many schemes exists for this purpose, such as the Jordan-Wigner transformation [Steudtner, 2019]. For the Lipkin model, an easier approach is available since the Hamiltonian can be written as products of the number and spin operators.

2.4 Variational Quantum Eigensolver

In this section we will briefly remind the reader of some key aspects of the variational method, followed by an outline on how observable values can be calculated using a QC.

2.4.1 Brief Remainder of the Variational Method

The Rayleigh-Ritz VM states that for a given Hamiltonian H, the expectation value of a *trial state* or *ansatz* $|A\rangle$ puts a lower bound on the ground state energy E_0.

$$\frac{\langle A|\, H\, |A\rangle}{\langle A|A\rangle} \geq E_0 \tag{7}$$

The ansatz is typically chosen to be a parameterized superposition of basis states that can be varied to improve the energy estimate, $|A\rangle \equiv |A(\boldsymbol{\theta})\rangle$ where $\boldsymbol{\theta} = (\theta_1, \ldots, \theta_M)$ are the M optimization parameters.

This is a crucial method in many-body theory, where good estimates of ground state energies are crucial due to the lack of analytical solutions. In contrast to perturbation theory, the VM will not give too small ground

state energies, assuming that the ansatz has some overlap with the true ground state. The VM machinery form the basis of the VQE.

2.4.2 Algorithm

We wish to apply the VM to estimate the ground state energy of a Hamiltonian on a quantum computer. To have any flexibility in the ansatz $|A\rangle$, we need to allow for parametrization. The most common approach is the so-called RY ansatz, where we apply chained operations of rotating around the y-axis (Eq. 5) by $\boldsymbol{\theta} = (\theta_1, \ldots, \theta_Q)$ of the Bloch sphere and CNOT operations (Eq. 4). Applications of y rotations specifically ensures that our coefficients always remain real, which often is satisfactory when dealing with many-body systems.
After the ansatz construction has been performed, the Hamiltonian must be applied. As discussed, the Hamiltonian must be written in terms of Pauli strings such that it is expressible as Eq. 6. To obtain the expectation value of the ground state energy, one can measure the expectation value of each Pauli string,

$$E(\boldsymbol{\theta}) = \sum_i w_i \langle A(\boldsymbol{\theta})| P_i |A(\boldsymbol{\theta})\rangle \equiv \sum_i w_i f_i,$$

where f_i is the expectation value of the Pauli string i. This is estimated statistically by considering measurements in the appropriate basis of the operator in the Pauli string. If the $P_i \supseteq Z_1$ we simply subtract the 0 and 1 outcomes of the first qbit, averaged over all measurements. If however we also have $P_i \supseteq X_2$, the second qbits measurement must be taken along the x-axis[1]. This with N_0 and N_1 as the number of 0 and 1 measurements respectively, we can estimate f_i since

$$f_i = \lim_{N\to\infty} \frac{N_0 - N_1}{N},$$

with N as the number of shots (measurements). Therefor each Pauli string requires it own circuit, where multiple measurements of each string is required. Adding the results together with the corresponding weights, the ground state energy can be estimated. To optimize wrt. $\boldsymbol{\theta}$, a classical optimizer is often applied. Gradients are estimated using a simple finite difference approximation

$$\nabla_{\boldsymbol{\theta}} E(\boldsymbol{\theta}) \approx \frac{E(\boldsymbol{\theta} + \delta\boldsymbol{\theta}) - E(\boldsymbol{\theta} - \delta\boldsymbol{\theta})}{2\delta\theta}, \tag{8}$$

where $\delta\boldsymbol{\theta} = (\delta\theta, \ldots, \delta\theta)$. By updating the previous $\boldsymbol{\theta}$ values with some scalar times the negative of the gradient estimate, a new set of $\boldsymbol{\theta}$ values are obtained. The process is then repeated a finite amount of steps, where we hope to converge to the global minimum. A schematic of the procedure is presented in Fig. 3.
An essential facet to this problem is the choice of an ansatz which will achieve a varied initial state, that can be altered through the optimization, furthering searches for better initial states. The ansatz used in this paper is shown in Fig(4), and is taken from the article by Hlatshwayo et al. Hlatshwayo et al. [2022]

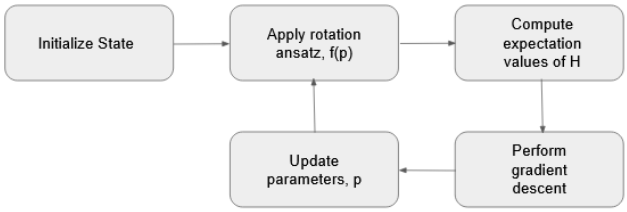

Figure 3: A schematic of the process of Variational Quantum Eigensolvers.

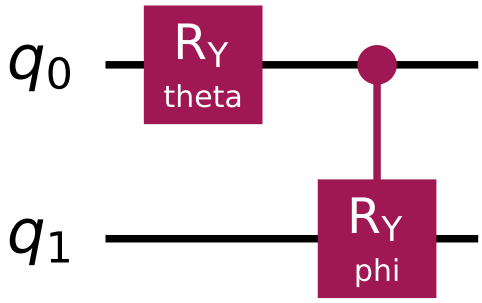

Figure 4: The ansatz for the VQE scheme applied for N = 4.

3 Quantum Systems

This section will introduce the three relevant systems for this work. Initially we will look at two 'toy models', being 2×2 and 4×4 real Hamiltonians with arbitrary entries. Lastly the Lipkin model will be used, showing many of the key features of many-body systems while still being analytically solvable.

3.1 $H \in \mathbb{R}^2$ Hamiltonian

As an initial test, we will consider a simply 2×2 real Hamiltonian consistend of a diagonal part H_0 and off-diagonal part H_I, playing the roles of a non-interactive one-body and interactive two-body part respectively. Defined through their matrix elements, we express them in the Pauli basis $\{|0\rangle, |1\rangle\}$

[1] To do this, we must must transform the qbit from the Pauli z-basis to the Pauli x-basis by application of a Hadamard gate.

$$
\begin{aligned}
H &= H_0 + H_I \\
H_0 &= \begin{pmatrix} E_1 & 0 \\ 0 & E_2 \end{pmatrix}, \qquad H_I = \lambda \begin{pmatrix} V_{11} & V_{12} \\ V_{21} & V_{22} \end{pmatrix}
\end{aligned} \tag{9}
$$

Where $\lambda \in [0, 1]$ is a coupling constant parameterizing the strength of the interaction.

3.2 $H \in \mathbb{R}^4$ Hamiltonian

We now move on to a slightly larger system, defined as a 4×4 real Hamiltonian. This can be viewed as two composite systems where each system is a two-level system. In the product basis $\{|00\rangle, |01\rangle, |10\rangle, |11\rangle\}$ we define the one-body part as

$$
H_0 |ij\rangle = \epsilon_{ij} |ij\rangle , \tag{10}
$$

with a two-body interaction defined using Pauli matricies

$$
\begin{aligned}
H_I &= H_x X \otimes X + H_z Z \otimes Z \\
&= \begin{pmatrix} H_z & 0 & 0 & H_z \\ 0 & -H_z & H_x & 0 \\ 0 & H_x & -H_z & 0 \\ H_x & 0 & 0 & H_z \end{pmatrix}
\end{aligned} \tag{11}
$$

Where H_x and H_y are couplings playing the same role as λ.

3.3 Lipkin Model

For larger many-body systems, the introduction of the occupation representation is common. The creation of a state p is represented by the operator $a_p^\dagger$, while annihilation a_p. Since we are dealing with fermions, the creation and annihilation operators follow the canonical anitcommutation relations

$$
\{a_p^\dagger, a_q^\dagger\} = \{a_p, a_q\} = 0, \quad \{a_p^\dagger, a_q\} = \delta_{pq}. \tag{12}
$$

The Lipkin model [Lipkin et al., 1965] for a N fermion system consists of two energy levels $\sigma \in \{\pm 1\}$, each having a degeneracy of N. Resembling fermionic half integer spin, the two levels contributes energetically $\pm\frac{1}{2}\epsilon$ for each particle. Additionally, we label the different states in each degenerate level by $p = 1, \dots N$ [2]. The Lipkin Hamiltonian can be written using creation and annihilation operators as

$$
\begin{aligned}
H &= H_0 + H_1 + H_2, \\
H_0 &= \frac{1}{2}\epsilon \sum_{pq} \sigma a_{p\sigma}^\dagger a_{p\sigma}, \\
H_1 &= \frac{1}{2} V \sum_{pp'\sigma} a_{p\sigma}^\dagger a_{p'\sigma}^\dagger a_{p'\bar{\sigma}} a_{p\bar{\sigma}}, \\
H_2 &= \frac{1}{2} W \sum_{pp'\sigma} a_{p\sigma}^\dagger a_{p'\bar{\sigma}}^\dagger a_{p'\sigma} a_{p\bar{\sigma}}.
\end{aligned} \tag{13}
$$

[2] This removes the spin quantum number from p, which commonly is included.

With $\bar{\sigma} = -\sigma$. H_0 is a diagonal single particle operator giving a contribution based on occupancy in the different levels. H_1 and H_2 are two-body operators moving pairs of particles between levels and exchanging particles between levels (spin-exchange) respectively. The strengths of these effects are parameterized by the couplings V and W. By defining the *quasi-spin* operators $J_\pm, J_z, J^2$ in addition to the number operator N as

$$
\begin{aligned}
J_\pm &= \sum_p a_{p\pm}^\dagger a_{p\mp} \\
J_z &= \frac{1}{2} \sum_{p\sigma} \sigma a_{p\sigma}^\dagger a_{p\sigma} \\
J^2 &= J_+ J_- + J_z^2 - J_z \\
N &= \sum_{p\sigma} a_{p\sigma}^\dagger a_{p\sigma}
\end{aligned} \tag{14}
$$

we can rewrite the Lipkin Hamiltonian from Eq. 13 using these

$$
\begin{aligned}
H_0 &= \epsilon J_z, \\
H_1 &= \frac{1}{2} V (J_+^2 + J_-^2), \\
H_2 &= \frac{1}{2} W (\{J_+, J_-\} - N),
\end{aligned} \tag{15}
$$

These quasi spin operators obey the normal spin commutator relations

$$
\begin{aligned}
[J_z, J_\pm] &= \pm J_\pm, & [J_+, J_-] &= 2J_z, \\
\left[J^2, J_\pm\right] &= 0, & \left[J^2, J_z\right] &= 0,
\end{aligned}
$$

in addition to commuting with the number operator

$$
[N, J_z] = [N, J_\pm] = \left[N, J^2\right] = 0.
$$

Using these relations we can show that the Hamiltonian (a product of quasi spin operators and the number operator) also commutes with J^2, that is $\left[H, J^2\right] = 0$. Therefor H and J^2 have shared eigenbasis, with J being a 'good' quantum number.

Using spin-eigenstates as the Hamiltonian basis, we define states through the normal approach $|J, J_z\rangle$ with J and J_z as spin and spin-projections respectively. The states $J_z = \pm J$ are the easiest to construct, corresponding to a single level being completely filled. States in between can then be found using the quasi-spin ladder operators following

$$
J_\pm |J, J_z\rangle = \sqrt{J(J+1) - J_z(J_z \pm 1)}\, |J, J_z \pm 1\rangle . \tag{16}
$$

Using this basis for the quasi-spin Hamiltonian from Eq. 15, the explicit matrix $H_{J_z, J_z'} = \langle J, J_z | H | J, J_z' \rangle$ can be constructed. For $N = 2$ particles, we have the triplet $J = 1$, with three possible projection $J_z = 0, \pm 1$. As

shown in App. .1, the Hamiltonian can be written in the J basis as

$$H = \begin{pmatrix} -\epsilon & 0 & V \\ 0 & W & 0 \\ V & 0 & \epsilon \end{pmatrix}. \tag{17}$$

By solving the eigenvalue problem, the ground state energy can be exactly found. Similarly, for the $N = 4$ case we have $J = 2$ with five possible projections $J_z = 0, \pm 1, \pm 2$. Using the same approach as in App. .1, the Hamiltonian can be expressed as

$$H = \begin{pmatrix} -2\epsilon & 0 & \sqrt{6}V & 0 & 0 \\ 0 & -\epsilon + 3W & 0 & 3V & 0 \\ \sqrt{6}V & 0 & 4W & 0 & \sqrt{6}V \\ 0 & 3V & 0 & \epsilon + 3W & 0 \\ 0 & 0 & \sqrt{6}V & 0 & 2\epsilon \end{pmatrix}. \tag{18}$$

To benchmark the VQE results for the Lipkin Model we will also compare with results from Hartree-Fock (HF) and random phase approximation (RPA). For the Lipkin Model these are also exactly solvable. From [Co' and De Leo, 2015] we have the Hartree-Fock solution

$$E_{\text{HF}} = -\frac{N}{2} \begin{cases} \epsilon + W & R < \epsilon \\ \frac{\epsilon^2 + (N-1)^2(V+W)^2}{2(N-1)(V+W)} + W & R > \epsilon, \end{cases} \tag{19}$$

which is split into two regions based on the relative strength between the interactions V, W and the single particle energies ϵ, $R \equiv (N-1)(V+W)$. Also from [Co' and De Leo, 2015], we have the RPA solution

$$E_{\text{RPA}} = E_{\text{HF}} + \frac{\omega - A}{2}, \tag{20}$$

where

$$\omega = \sqrt{A^2 - |B|^2}.$$

The coefficients A and B are region specific, explicitly

$$A = \begin{cases} \epsilon - (N-1)W & R < \epsilon \\ \frac{3(N-1)^2(V+W)^2 - \epsilon^2}{2(N-1)(V+W)} - (N-1)W & R > \epsilon, \end{cases}$$

$$B = \begin{cases} -(N-1)V & R < \epsilon \\ -\frac{\epsilon^2 + (N-1)^2(V+W)^2}{2(N-1)(V+W)} + (N-1)W & R > \epsilon. \end{cases}$$

3.4 Encodings

3.4.1 Toy Hamiltonians

Firstly we need to express the Hamiltonian from Eq. 9 using Pauli matrices. Beginning with the diagonal H_0, we need to fill the both entries with different energy values. Defining their difference using

$$E_+ = \frac{E_1 + E_2}{2}, \qquad E_- = \frac{E_1 - E_2}{2}$$

we see that by combining the identity and Z Pauli matrix, this can be expressed as

$$H_0 = E_+ I + E_- Z$$

For H_1 we use the same trick to fill the diagonal, defining $V_+ = (V_{11} + V_{22})/2, V_- = (V_{11} - V_{22})/2$. From the hermiticity requirements of H, we note that $V_{12} = V_{21} \equiv V_o$, which simplifies the problem to a simple X. Therefor

$$H_I = V_+ I + V_- Z + V_o X$$

For the 4×4 case we note that the interacting part of the Hamiltonian Eq. 10 is already written in terms of Pauli matrices, and no encoding beyond this is necessary. The diagonal however needs to be rewritten. Following the same procedure as the 2×2 case, we define

$$\epsilon_{\pm 0} = \frac{\epsilon_{00} \pm \epsilon_{01}}{2}, \qquad \epsilon_{\pm 1} = \frac{\epsilon_{10} \pm \epsilon_{11}}{2}.$$

We note that the energies ϵ_{00} and ϵ_{01} can be repeated on the diagonal, and the same for ϵ_{10} and ϵ_{11}

$$D_0 = \epsilon_{+0} I \otimes I + \epsilon_{-0} I \otimes Z,$$
$$D_1 = \epsilon_{+0} I \otimes I + \epsilon_{-1} I \otimes Z.$$

One qbit project operators can also be constructed considering I and Z through

$$P_\pm = \frac{1}{2}(I \pm Z)$$

which we expand to the project out the first and last to two elements of 4×4 matrix

$$P_0 = P_+ \otimes I, \qquad P_0 = P_- \otimes I.$$

Then by adding D_0 and D_1, while project out the irrelevant parts, we find

$$\begin{aligned} H_0 &= P_0 D_0 + P_1 D_1, \\ &= \alpha_+ I \otimes I + \alpha_- Z \otimes I + \beta_+ I \otimes Z + \beta_- Z \otimes Z, \end{aligned}$$

where we have defined

$$\alpha_\pm = \frac{\epsilon_{+0} \pm \epsilon_{+1}}{2}, \quad \beta_\pm = \frac{\epsilon_{-0} \pm \epsilon_{+1}}{2}$$

3.4.2 Lipkin Model

Using the level mapping from [Hlatshwayo et al., 2022], the spin operators from Eq. 14 can be written using their one-body counterparts

$$J_z = \sum_i^N j_z^{(i)} \qquad J_\pm = \sum_i^N j_\pm^{(i)} = \sum_i^N (j_x^{(i)} \pm i j_y^{(i)}) \quad (21)$$

with N being the number of particles. Additionally, since we have spin-$^1/_2$ fermions, the mapping to Pauli matrices follow

$$j_x^{(i)} = \frac{1}{2} X_i, \qquad j_y^{(i)} = \frac{1}{2} Y_i, \qquad j_z^{(i)} = \frac{1}{2} Z_i. \quad (22)$$

This means that we require N qbits to calculate properties of a N particle system, if no more symmetry reductions are considred. As shown in App. .2, Eq. 15 can be expressed as

$$\begin{aligned} H_0 &= \frac{\epsilon}{2} \sum_p Z_p, \\ H_1 &= \frac{1}{2} V \sum_{p<q} X_p X_q - Y_p Y_q, \\ H_2 &= \frac{1}{2} W \sum_{p<q} (X_p X_q + Y_p Y_q). \end{aligned} \quad (23)$$

We will investigate the integer spin systems $N = 2$ $(J = 1)$ and $N = 4$ $(J = 2)$. Writing out the expressions from Eq. 23 we have for two particles

$$H^{N=2} = \frac{\epsilon}{2} (Z_1 + Z_2) + \frac{W+V}{2} X_1 X_2 - \frac{W-V}{2} Y_1 Y_2 \quad (24)$$

and for four particles

$$\begin{aligned} H^{N=4} =& \frac{\epsilon}{2} (Z_1 + Z_2 + Z_3 + Z_4) + \frac{W-V}{2} \Big(X_1 X_2 + \\ & X_1 X_3 + X_1 X_4 + X_2 X_3 + X_3 X_4 + X_3 X_4 \Big) \\ & + \frac{W+V}{2} \Big(Y_1 Y_2 + Y_1 Y_3 + Y_1 Y_4 + Y_2 Y_3 \\ & + Y_3 Y_4 + Y_3 Y_4 \Big) \end{aligned} \quad (25)$$

Which is quite a mouthful. If we set $W = 0$, reductions of the problem can be performed. Looking back at Eq. 15, we note that if only H_0 and H_1 are included, spins differing by ± 2 are the only possible non-diagonal couplings. Since H_0 is diagonal and single particle energies are degenerate, it does not break the pairing symmetry. Instead of the $2J + 1$ spin projections, we simply have $J + 1$ relevant states. From [Hlatshwayo et al., 2022] we have the two-qbit Hamiltonian for $N = 4$ as

$$H_{W=0}^{N=4} = \epsilon (Z_1 + Z_2) + \frac{\sqrt{6}}{2} V (X_1 + X_2 + Z_1 X_0 - X_1 Z_0). \quad (26)$$

This will be more computationally efficient due to requiring only half the qbits of Eq. 25. Both schemes will be applied.

3.5 Calculating density matrices

Given a Hamiltonian consisting of a non- and an interacting Hamiltonian on a two qubit state, a state will have eigenvectors with coefficients α_{ij}. For a Hamiltonian, which in matrix form has 4×4 dimension, there will be four sets of eigenvectors, given a representation of the states in the form

$$|00\rangle = \begin{pmatrix} 1 & 0 & 0 & 0 \end{pmatrix}^T \quad (27)$$

$$|01\rangle = \begin{pmatrix} 0 & 1 & 0 & 0 \end{pmatrix}^T \quad (28)$$

$$|10\rangle = \begin{pmatrix} 0 & 0 & 1 & 0 \end{pmatrix}^T \quad (29)$$

$$|11\rangle = \begin{pmatrix} 0 & 0 & 0 & 1 \end{pmatrix}^T \quad (30)$$

The resulting density matrix, will be the outer product of each of these eigenstates of the Hamiltonian. The density matrix can be decomposed into partial density matrices describing the separate Hilbert space of one of the qubits, by partially tracing over the other qubit. This is done in the below calculation.

$$\begin{aligned} \rho = \alpha_{00} |00\rangle \langle 00| + \alpha_{01} |01\rangle \langle 01| + \alpha_{10} |10\rangle \langle 10| \\ + \alpha_{11} |11\rangle \langle 11| \\ \rho_A = Tr_B(\rho) = \big(\boldsymbol{I} \otimes \langle \psi| \big) \, \rho \big(\boldsymbol{I} \otimes |\psi\rangle \big) \\ \rho_B = Tr_A(\rho) = \big(\langle \psi| \otimes \boldsymbol{I} \big) \, \rho \big(|\psi\rangle \otimes \boldsymbol{I} \big) \end{aligned}$$

With the state $|\psi\rangle = \frac{1}{\sqrt{2}}(|0\rangle + |1\rangle)$, the resulting reduced density matrix ρ_A and ρ_B is

$$\begin{aligned} \rho_A &= \frac{1}{2} \Big(\alpha_{00} |0\rangle \langle 0| + \alpha_{01} |0\rangle \langle 0| + \alpha_{10} |1\rangle \langle 1| + \alpha_{11} |1\rangle \langle 1| \Big) \\ &= \frac{1}{2} \Big(\big(\alpha_{00} + \alpha_{01} \big) |0\rangle \langle 0| + \big(\alpha_{10} + \alpha_{11} \big) |1\rangle \langle 1| \Big) \quad (31) \\ \rho_B &= \frac{1}{2} \Big(\alpha_{00} |0\rangle \langle 0| + \alpha_{01} |1\rangle \langle 1| + \alpha_{10} |0\rangle \langle 0| + \alpha_{11} |1\rangle \langle 1| \Big) \\ &= \frac{1}{2} \Big(\big(\alpha_{00} + \alpha_{10} \big) |0\rangle \langle 0| + \big(\alpha_{01} + \alpha_{11} \big) |1\rangle \langle 1| \Big) \quad (32) \end{aligned}$$

The von Neumann entanglement entropy is defined by the trace of the product between the reduced density matrix and the logarithm of the reduced density matrix. Using Eq. (31) we get

$$S(\rho_i) = - Tr \Big(\rho_i \ln \rho_i \Big) \quad (33)$$

$$\begin{aligned} \implies S(\rho_a) =& \frac{\ln 2}{2} \Big(\big(\alpha_{00} + \alpha_{10} \big) \times \big(\alpha_{01} + \alpha_{11} \big) \Big) \quad (34) \\ & \times \ln \big(\alpha_{00} + \alpha_{10} \big) \times \ln \big(\alpha_{01} + \alpha_{11} \big) \end{aligned}$$

It quantizes the entanglement between the two separate Hilbert spaces. The maximal entropy for a two qubit mixed state, will be $\ln 2$, that of a Bell state. This leads

to a possible visualization of the entanglement von Neumann entropy as a metric of the "probability" of achieving a Bell state, given a mixed state, normalized by $\ln 2$. This generalizes for more qubits, it is a measure of the "probability" of achieving maximally entangled states.

4 Results

The code developed during this project is openly available at `github.com/hkve/Lipkin-Model-FYS5419`. Viewer discretion is advised.

4.1 Toy Models

The energy eigenstates and $\{|0\rangle, |1\rangle\}$ coefficients for the $H \in \mathbb{R}^2$ Hamiltonian as a function of interaction strength λ is shown in figure Fig. 5. Despite having two free parameters C_0, C_1 they are constrained through normalization.

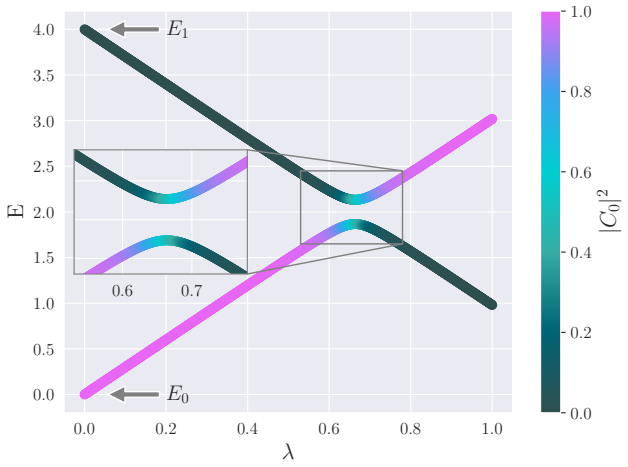

Figure 5: Energy eigenstates and coefficients of 2×2 Hamiltonian when varying the interaction strength $\lambda \in [0, 1]$. Calculations done using exact diagonalization.

The results of using VQE on the simple 2×2 Hamiltonian is presented in Fig. 6. It is the lower section of Fig. 5 extracted for comparison with VQE. It correctly predicts the ground state energy for this simple Hamiltonian, verifying the precision of the method for basic usage. This is an essential step in developing the system for more complex Hamiltonians and systems, which follows.

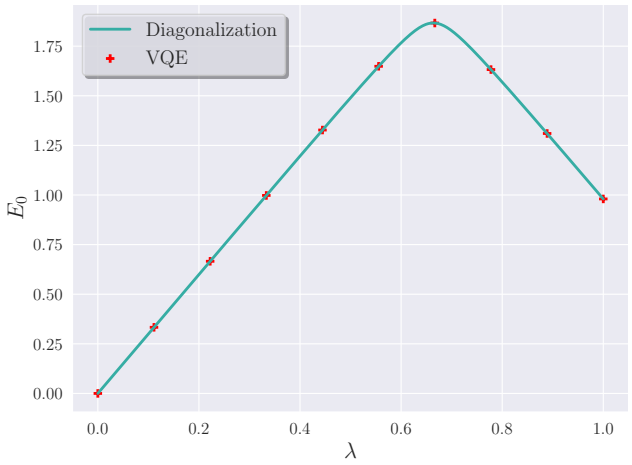

Figure 6: Showing ground state energy of the 2×2 Hamiltonian, calculated using diagonalization and the VQE for $\lambda \in [0, 1]$.

The slightly larger 4×4 Hamiltonian ground state energy calculated using VQE is shown in Fig. 7. Again we see a good correspondence between the diagonalization and our VQE calculations.

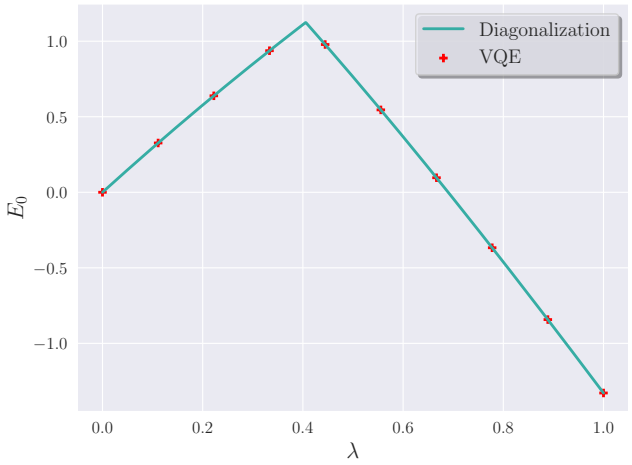

Figure 7: Showing ground state energy of the 4×4 Hamiltonian, calculated using diagonalization and the VQE for $\lambda \in [0, 1]$.

The entropy of entanglement in the case of the of the Hamiltonian consisting of a interacting and non-interacting between the two states, is presented in Fig. (8). It is apparent that the entropy of entanglement increases as the connection strength increases. The entropy of entanglement converges when the interaction strength thoroughly dominates the non-interaction contribution.

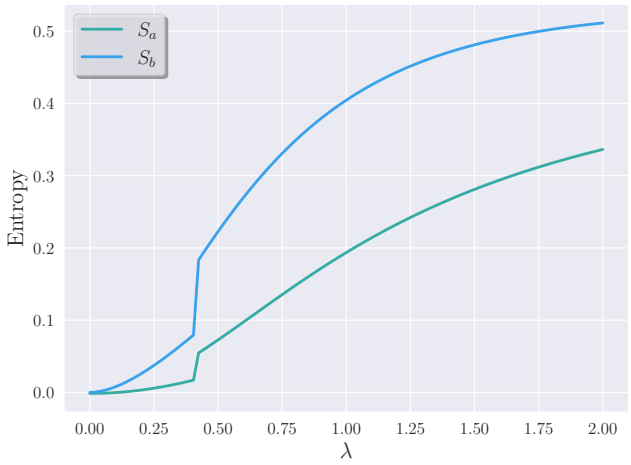

Figure 8: The von Neumann entanglement entropy of the subsystems A and B, as a function of interaction strength, λ

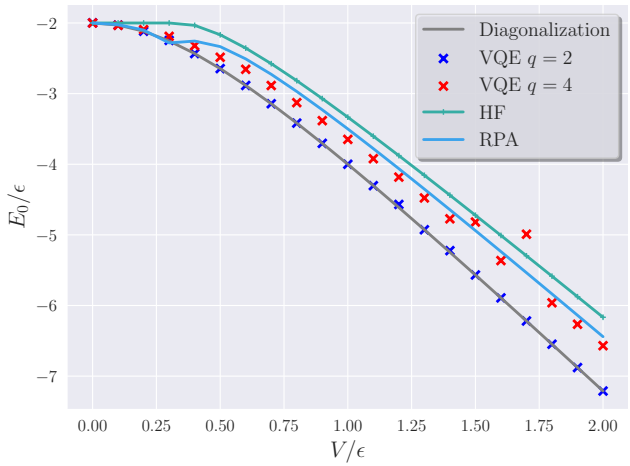

Figure 10: Ground state values for the Lipkin model for $N = 4$ particles with $W = 0$ as a function of V/ϵ. Calculations were done using exact diagonalization, VQE for both two (Eq. 26) and four (Eq. 25) qbits, in addition to closed form HF and RPA expressions. The two and four qbit cases were calculated using 300 and 1000 iterations respectively.

4.2 Lipkin Model

For the Lipkin Model, we initially investigate the $W = 0$ case. For the two particles, we apply the VQE where two qbits are required, one for each particle Eq. 24. Additionally, we compare with the HF Eq. 19 and RPA Eq. 20. This is shown as a function of V/ϵ in Fig. 9

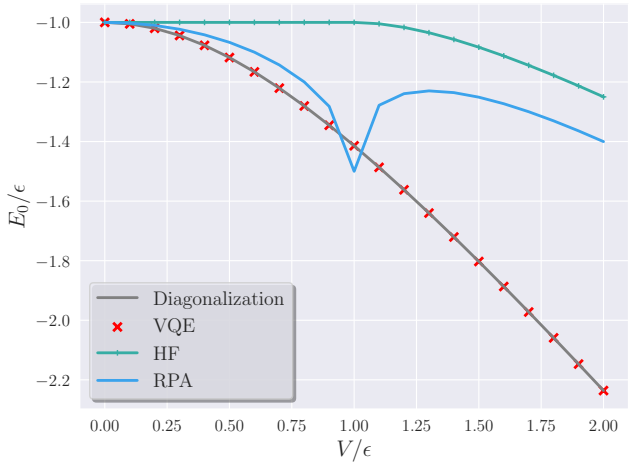

Figure 9: Ground state values for the Lipkin model for $N = 2$ particles with $W = 0$ as a function of V/ϵ. Calculations were done using exact diagonalization, VQE with 30 iterations, in addition to closed form HF and RPA expressions.

Moving on to the four particle case, but still keeping $W = 0$, we present the energy as a function of V/ϵ in Fig. 10. Here we have used both the $Q = 4$ (Eq. 25) and the $Q = 2$ (Eq. 26) Hamiltonians. In addition, we also compare with HF and RPA solutions.

Lastly we lift the $W = 0$ restriction for four particles and consider the ground state energy as a function of both V/ϵ and W/ϵ. In Fig. 11a we see the relative error from the diagonalization results. Additionally, we benchmark this against the HF and RPA solutions shown in Fig. 11b and Fig. 11c respectively.

5 Discussion

5.1 Toy models

Going back to Fig. 5 we see the classical example of level crossing in two-level systems. The phenomenon gets its name because in a plot of energy versus interaction strength, the energy levels appear to cross or avoid crossing each other, depending on the specific parameters and interactions involved, as seen. Taking a look at the coefficients, we see that for small interaction strengths λ, the ground state and excited state are almost purely dominated by $|0\rangle$ and $|1\rangle$ respectively. Increasing λ, the domination is less and less present. This continues until we reach $\lambda = 2/3$, where the ground state energy is maximal and excitation energy minimal. Moving past $\lambda = 2/3$ results in the ground state being dominated by $|1\rangle$ and the excited state by $|0\rangle$, meaning that the states has change or swapped character.

The ground state calculation using the VQE for the two toy models resulted in precise results, as shown in Fig. 6 (2×2) and Fig. 7 (4×4). By optimizing for $\sim$ 1000 iterations, the variability across different runs were minuscule. However, for a lower number of iterations, the accuracy for the two qbit systems was in general worse than the single qbit system, as would be expected. These

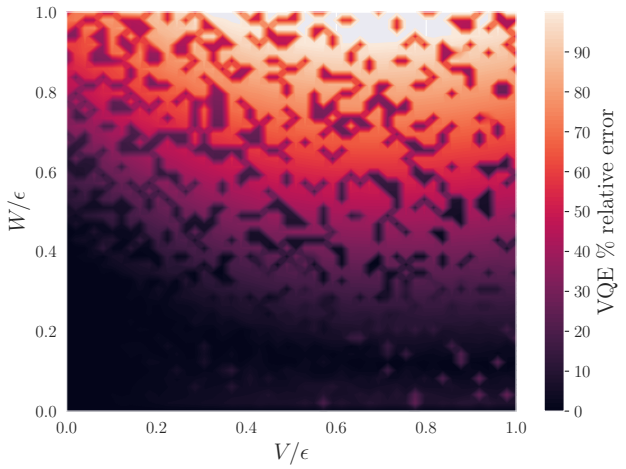

(a) Variational Quantum Eigensolver. All energies were calculated using 1000 iterations.

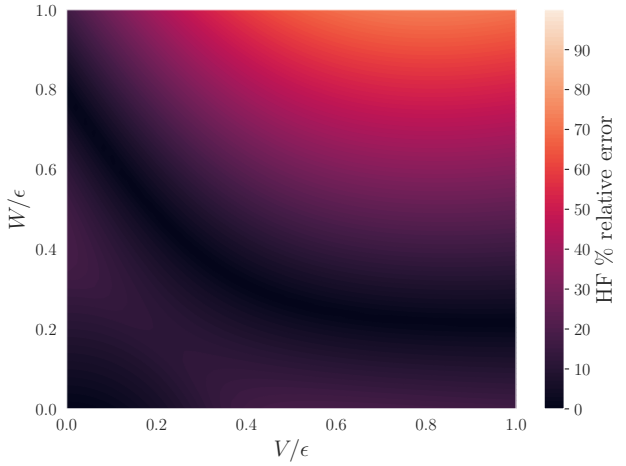

(b) Hartree-Fock, closed form expressions

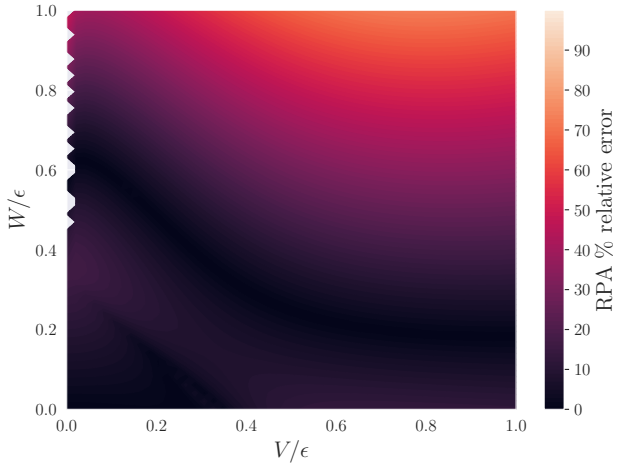

(c) Random Phase Approximation, closed form expressions

Figure 11: Relative error in ground state energy for the Lipkin model, using $N = 4$ particles as a function of V/ϵ and W/ϵ.

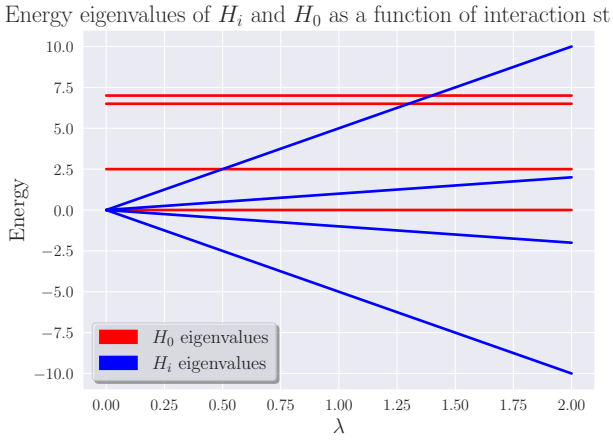

Figure 12: The eigenvalues of the interaction and non-interaction Hamiltonian, as a function of connection strength λ.

initial tests served as a good benchmark to validate our further Lipkin results.

5.2 Entropy

The entropy in Fig. (8) has an initial contribution which increases slower, before taking a leap for a connection strength of $\lambda \approx 0.4$. This is probably a jump corresponding to a system being slightly interacting into being entangled. The entanglement further increases before converging around $\lambda \approx 1.3$. Studying Fig(12) we can extract some information, seeing as the first jump is correlated with the eigenvalues of the interaction Hamiltonian overcoming the second lowest eigenvalues. The convergence can be interpreted as the interaction energy overcoming the higher eigenvalues of the non-interaction Hamiltonian.

From Figs. (13a) and (13b) the situation of the first spike in increased entropy from Fig. (8) is visualized through the diagonal of the reduced density matrices of the two sub-systems. It is apparent that there occurs a switch around $\lambda = 0.4$ where the reduced density matrices swaps from being in the state

$$\rho_a(\lambda = 0.3) = c_1 \left|0\right\rangle \left\langle 0\right| \rightarrow \rho_a(\lambda = 0.5) = c_2 \left|1\right\rangle \left\langle 1\right|$$

There is a similar occurence in the reduced density matrix of ρ_b. These are not pure states, implicated by the trace of the diagonal, but the system of ρ_a is more diagonalized, which makes it stricter in the outcomes of its entanglement, whereas ρ_b has low occurrences along the diagonal, implicating that there are larger mixtures of states, which is more ideal for entanglement. Thus implicating the higher entropy for ρ_b in Fig. (8). This is further emphasized when studying Fig(14). Here the connection strength dominates, which is indicated by the "weak" amplitude of the density matrices of the two

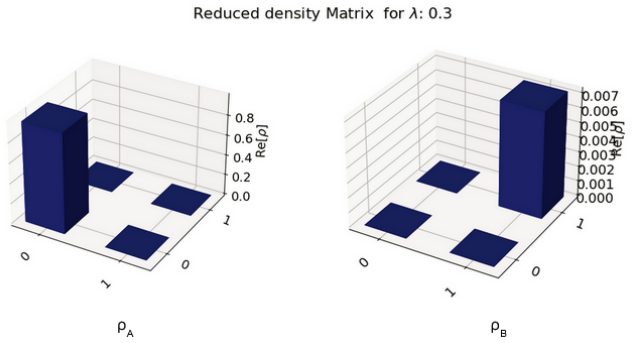

(a) The reduced density matrix of ρ_a and ρ_b for a interaction strength of $\lambda = 0.3$

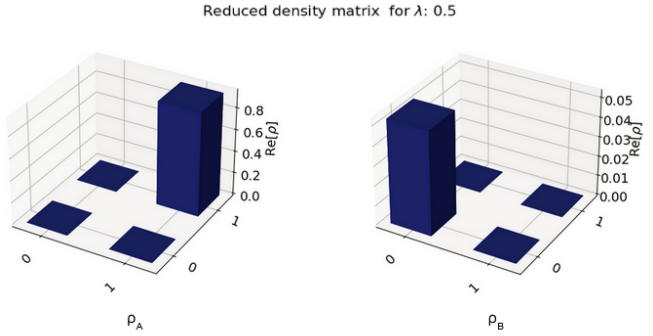

(b) The reduced density matrix of ρ_a and ρ_b for a interction strength of $\lambda = 0.5$

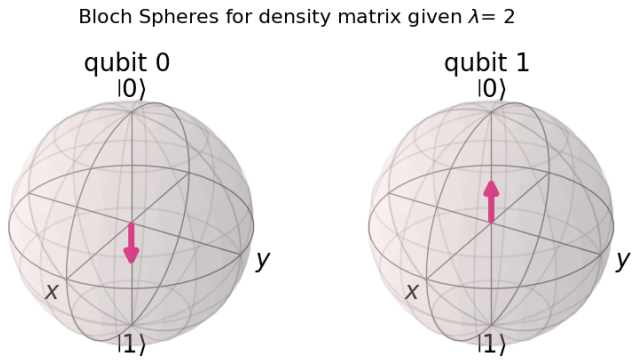

Figure 14: The Bloch-spheres of the two qubits given $\lambda = 2$.

states, which implies a superposition of states. These have higher entanglement than pure states which have amplitudes on the vectors stretching to the sphere.

5.3 Lipkin Model

From Fig. 9 we see good agreement between diagonalization and VQE. There were little trouble with convergence and precise results were obtained after just 30 iterations. The variability between runs were also minuscule, except when running for less than 30 iterations. It is also clear that VQE beats both HF and RPA consistently for the range of interaction strengths.

Moving on to the four particle case from Fig. 10, the precision of the results decreases. The two qbit scheme making use of the $W = 0$ symmetry still shows excellent agreement with the diagonalization, but the larger four qbit scheme performs worse. This was the case despite increasing the number of iterations to 1000. Still, the four qbit results outperformed both HF and RPA for all except two interaction strengths, but showed some variability in results across identical runs. We hypothesize multiple reasons for this. Firstly, the number of Pauli string from Eq. 25 is 16 compared to the encoding from Eq. 26 only containing 6. We are therefor reliant on good estimates of Pauli string expectation values for more terms. If one or more of these estimates are poor for one iteration, the gradient estimate or the energy evaluation itself could be erroneously, resulting in slower converge. Intertwined with this is the sice of the parameter space which is twice as large for the four qbit case. Optimization here is harder and could hinder the convergence of the VQE. The RY ansatz could of course also be too naive, restricting to only real amplitudes. Various different approaches are present in the literature, for instance the popular Unitary Coupled Cluster [Peruzzo et al., 2014] being one of the gold standards in quantum chemistry. The runtime also increased with more qbits as expected. This is a clear indication that spending time reducing the number of Pauli strings by considering the symmetries of the system at hand is a worthwhile task.

When lifting the $W = 0$ restriction, such as we saw in Fig. 11a, the convergence trouble was more apparent. For low W values, the VQE outperformed both HF and RPA from Fig. 11b and Fig. 11c respectively. For $V \to \epsilon$ but still $W \ll \epsilon$ some runs ended at $\sim 30\%$ relative error, but mostly the ground state was accurately estimated. Considering low V values, accurate results can be seen up until $W \approx \epsilon/2$, before convergence reduces. The middle regions $W, V \in [0, \epsilon/3]$ seems to be the area where VQE would be clearly preferred over HF and RPA. This means we can handle systems where the interaction plays a relatively large part Hamiltonian, but not highly interactive systems.

The results from Fig. 11a are quite perforated, indicat-

ing that better results could be achieved by increasing the number of iterations and/or running each set of (V, W) values multiple times. However since we are simulating a QC, simulating repeated VQE calculations for four qbit system for a range of different Hamiltonian would be too time-consuming for this work. Alternatively trying to find new clever ways to rewrite the Pauli strings Eq. 25 could be worthwhile, in addition to testing different ansatzes.

Moving forward, calculations of other observable than the energy for ground state would be interesting. While the VQE is primarily focused on energy estimation, it can also yield approximate estimates for other observables, especially if they are closely related to the energy. This is because the optimized trial state tends to capture some aspects of the true state, which can influence the values of other observables. However, the accuracy of these estimates may vary depending on the specific system and observable of interest.

5.4 Future research

The decision of the ansatz in Fig. (4) seems a bit arbitrary, but is based on the ansatz in Hlatshwayo et al. (Hlatshwayo et al. [2022]). There could be possibilities in optimization by choosing a different ansatz. This would be a section of further research by delving into a review of VQE by Tilly et al. (Tilly et al. [2022]).
Further research could look into other methods of optimization, other than the VQE algorithm, as it is a fairly simple model with restricted applicability. It could probably be extended to solving other optimization problems with minor tweaks or clever encoding. The Lipkin model is fairly limited when it comes to QC. This is a result of the angular momentum operators j_+ and j_- are not unitary and thus not applicable to general QC. Thus other models could be further researched in order to not simplify the Hamiltonian by non-unitarity. These models become fairly complex quickly and involves heavier computational costs in order to construct and optimize.

6 Concluding remarks

A simple 2×2 Hamiltonian consisting of a interacting and non-interacting part has been modelled and the lowest energy of this Hamiltonian has been compared to the results of the VQE algorithm for varying degrees of interaction strength, ranging from $\lambda \in [0, 1]$. VQE is very well equipped for this problem, yielding satisfying results. For a two qubit system, the Hamiltonian becomes more complex. The ground state energy of the systems was again precisely estimated using the VQE, with little variability across runs.
For the 4x4 Hamiltonian of the two qubit system the entanglement entropy was found to be increasing as a result of larger connection strength. The reduced density matrices of the system is less pure and under interaction and will create a strong entanglement when the energy of interaction surpasses that of the non-interaction Hamiltonian.
For the Lipkin model with $W = 0$ we find good correspondence when using the RY ansatz for the two qbit schemes, outperforming HF and RPA for two and four particles across a range of interaction strengths. Using the $Q = N$ scheme for four particles yielded more variability, demonstrating that reducing complexity of Pauli strings and encoding schemes not only reduce computational time but also increase precision. Considering $W, V > 0$, low to medium interaction strengths up to $\sim \epsilon/3$ outperformed RPA and HF. For highly interactive systems, convergence to good ground state energies was more difficult. Exploring the dependency on different types of ansatz choices could improve the results for stronger interactions.

7 Appendix

.1 $J = 1$ Lipkin Hamiltonian

Since we have expressed the Hamiltonian using quasi-spin operators, investigating how the states $|J, J_z\rangle$ are related to each other will be beneficial. For $J = 1$ ($N = 2$) we can write the $J_z = \pm 1$ states as

$$|1, \pm 1\rangle = a^\dagger_{1\pm} a^\dagger_{2\pm} |0\rangle$$

The states are related to each other, in additon to the third $|1, 0\rangle$ states through Eq. 16.

$$\begin{aligned} J_+ |1,-1\rangle &= \sqrt{2}\,|1,0\rangle & J_- |1,-1\rangle &= 0 \\ J_+ |1,0\rangle &= \sqrt{2}\,|1,1\rangle & J_- |1,0\rangle &= \sqrt{2}\,|1,-1\rangle \\ J_+ |1,1\rangle &= 0 & J_- |1,1\rangle &= \sqrt{2}\,|1,0\rangle \end{aligned}$$

Inspecting Eq. 15 we see that H_0 only acts on the diagonal

$$\langle J, J_z | H_0 | J, J'_z \rangle = \epsilon J_z \delta_{J_z, J'_z}$$

In addition, the pair mover, as the name entails, only if there are states differing by two units of angular momentum since H_1 contains $J^2_\pm$. We see that

$$\begin{aligned} \langle J, J_z | H_1 | J, J_z \pm 2\rangle &= \frac{1}{2} V \langle J, J_z | J^2_\mp | J, J_z \pm 2\rangle \\ &= \frac{1}{2} V (\sqrt{2})^2 \langle J, J_z | J, J_z\rangle = V \end{aligned}$$

Lastly H_2 have $J_\pm J_\mp$ and N terms contributing for all diagonal terms. For $|1, \pm 1\rangle$, these cancel out since

$$\begin{aligned} \langle 1, \pm 1 | J_\pm J_\mp | 1, \pm 1\rangle &= 2 \\ \langle 1, \pm 1 | N | 1, \pm 1\rangle &= 2 \end{aligned}$$

But for $|1, 0\rangle$ we get a contribution from both $J_+ J_-$ and $J_- J_+$, giving a total contribution off

$$\begin{aligned} \langle 1, 0 | H_2 | 1, 0\rangle &= \frac{1}{2} W \langle 1, 0 | J_+ J_- + J_- J_+ - N | 1, 0\rangle \\ &= \frac{1}{2} W (2 + 2 - 2) = W \end{aligned}$$

Combining these results we find

$$H = \begin{pmatrix} -\epsilon & 0 & V \\ 0 & W & 0 \\ V & 0 & \epsilon \end{pmatrix}$$

Ordered such that $\langle J, J_z | H | J, J'_z \rangle = H_{J_z+1, J'_z+1}$

.2 Detailed Pauli Encoding of the Lipkin Model

We will now convert Eq. 14 to Eq. 23 using the spin mappings from Eq. 21 and Eq. 22. The diagonal term H_0 is quite simple, where we simply substitute in for the z spin giving

$$H_0 = \epsilon J_z = \epsilon \sum_p j_z^{(p)} = \frac{\epsilon}{2} \sum_p Z_p$$

Moving on to the H_1 term, we need to expand the square of the $J_\pm$ operators. Starting with J_+ we find

$$\begin{aligned} J^2_+ &= \left(\sum_p j_x^{(p)} + i j_y^{(p)} \right)^2 = \sum_{pq} \left(j_x^{(p)} + i j_y^{(p)} \right) \left(j_x^{(q)} + i j_y^{(q)} \right) \\ &= \sum_{pq} j_x^{(p)} j_x^{(q)} - j_y^{(p)} j_y^{(q)} + i j_y^{(p)} j_x^{(q)} + i j_x^{(p)} j_y^{(q)} \end{aligned} \tag{.1}$$

Similarly, the J^2_- term yields

$$J^2_- = \sum_{pq} j_x^{(p)} j_x^{(q)} - j_y^{(p)} j_y^{(q)} - i j_y^{(p)} j_x^{(q)} - i j_x^{(p)} j_y^{(q)}. \tag{.2}$$

By inspection we see that the cross terms of Eq. .1 and Eq. .2 cancel each other. We can then expand in diagonal and off-diagonal terms and substitute in the mapping from Eq. 22.

$$\begin{aligned} J^2_+ + J^2_- &= 2 \sum_{pq} j_x^{(p)} j_x^{(q)} - j_z^{(p)} j_z^{(q)} \\ &= 2 \sum_p (j_x^{(p)})^2 - (j_y^{(p)})^2 + 4 \sum_{p>q} j_x^{(p)} j_x^{(q)} - j_y^{(p)} j_y^{(q)} \\ &= \frac{1}{2} \sum_p X_p^2 - Y_p^2 + \sum_{p>q} X_p X_q - Y_p Y_q \end{aligned}$$

The diagonal term will cancel out, since the Pauli matrices are involutory, giving the pair moving Hamiltonian

$$H_1 = \frac{1}{2} V \sum_{p>q} X_p X_q - Y_p Y_q \tag{.3}$$

Lastly for H_2, we need to calculate the mixing terms of $J_\pm$ operators from Eq. 15. Following the same procedure we see that

$$\begin{aligned} J_+ J_- &= \left(\sum_p j_x^{(p)} + i j_y^{(p)} \right) \left(\sum_p j_x^{(p)} - i j_y^{(p)} \right) \\ &= \sum_{pq} j_x^{(p)} j_x^{(q)} + j_y^{(p)} j_y^{(q)} - i j_x^{(p)} j_y^{(q)} - i j_y^{(p)} j_x^{(q)} \end{aligned}$$

Similarly the other mixing term gives

$$\begin{aligned} J_- J_+ &= \left(\sum_p j_x^{(p)} - i j_y^{(p)} \right) \left(\sum_p j_x^{(p)} + i j_y^{(p)} \right) \\ &= \sum_{pq} j_x^{(p)} j_x^{(q)} + j_y^{(p)} j_y^{(q)} + i j_x^{(p)} j_y^{(q)} + i j_y^{(p)} j_x^{(q)} \end{aligned}$$

Again we see that the cross terms of $j_x^{(p)}$ and $j_y^{(q)}$ cancel out. Expanding in diagonal and off-diagonal terms

$$\begin{aligned}\{J_+, J_-\} &= 2\sum_{pq} j_x^{(p)} j_x^{(q)} + j_y^{(p)} j_y^{(q)} \\ &= 4\sum_{p<q} j_x^{(p)} j_x^{(q)} + j_y^{(p)} j_y^{(q)} + 2\sum_p \left(j_x^{(p)}\right)^2 + \left(j_y^{(q)}\right)^2\end{aligned}$$

And inserting the mapping to Pauli matrices Eq. 22 we find

$$\begin{aligned}\{J_+, J_-\} &= \sum_{p<q} X_p X_q + Y_p Y_q + \frac{1}{2}\sum_p X_p^2 + Y_p^2 \\ &= \sum_{p<q} (X_p X_q + Y_p Y_q) + I\end{aligned}$$

From Eq. 15 we see that H_2 contains the diagonal number operator, which simply is the identity canceling the identity from $\{J_+, J_z\}$

$$H_2 = \frac{1}{2} W \sum_{p<q} X_p X_q + Y_p Y_q \tag{.4}$$

References

Giampaolo Co' and Stefano De Leo. Hartree-fock and random phase approximation theories in a many-fermion solvable model. *Modern Physics Letters A*, 30(36):1550196, November 2015. ISSN 0217-7323. doi: 10.1142/S0217732315501965. URL https://www.worldscientific.com/doi/abs/10.1142/S0217732315501965. Publisher: World Scientific Publishing Co.

Manqoba Q. Hlatshwayo, Yinu Zhang, Herlik Wibowo, Ryan LaRose, Denis Lacroix, and Elena Litvinova. Simulating excited states of the Lipkin model on a quantum computer. *Physical Review C*, 106(2): 024319, August 2022. doi: 10.1103/PhysRevC.106.024319. URL https://link.aps.org/doi/10.1103/PhysRevC.106.024319. Publisher: American Physical Society.

H. J. Lipkin, N. Meshkov, and A. J. Glick. Validity of many-body approximation methods for a solvable model: (I). Exact solutions and perturbation theory. *Nuclear Physics*, 62(2):188–198, February 1965. ISSN 0029-5582. doi: 10.1016/0029-5582(65)90862-X. URL https://www.sciencedirect.com/science/article/pii/002955826590862X.

Alberto Peruzzo, Jarrod McClean, Peter Shadbolt, Man-Hong Yung, Xiao-Qi Zhou, Peter J. Love, AlÃ¡n Aspuru-Guzik, and Jeremy L. O'Brien. A variational eigenvalue solver on a quantum processor. *Nature Communications*, 5(1):4213, July 2014. ISSN 2041-1723. doi: 10.1038/ncomms5213. URL http://arxiv.org/abs/1304.3061. arXiv:1304.3061 [physics, physics:quant-ph].

M. Steudtner. *Methods to simulate fermions on quantum computers with hardware limitations*. PhD thesis, Leiden, November 2019. URL https://hdl.handle.net/1887/80413. ISBN: 9789085934165.

Jules Tilly, Hongxiang Chen, Shuxiang Cao, Dario Picozzi, Kanav Setia, Ying Li, Edward Grant, Leonard Wossnig, Ivan Rungger, George H. Booth, and Jonathan Tennyson. The variational quantum eigensolver: A review of methods and best practices. *Physics Reports*, 986:1–128, nov 2022. doi: 10.1016/j.physrep.2022.08.003. URL https://doi.org/10.1016%2Fj.physrep.2022.08.003.